RSC Sustainability

PAPER

View Article Online
View Journal | View Issue

Cite this: *RSC Sustainability*, 2026, 4, 1062

Sustainable chemical recycling of low-density polyethylene into light olefins over nano-sized SSZ-13

Yoshiki Murata,[a] Ryuga Nakai,[a] Koji Miyake, *[ab] Yoshiaki Uchida,[a] Atsushi Mizusawa,[c] Tadashi Kubo[c] and Norikazu Nishiyama[ab]

Received 19th July 2025
Accepted 15th December 2025

DOI: 10.1039/d5su00602c

rsc.li/rscsus

As the demand for sustainable resource utilization increases, chemical recycling of plastic waste is emerging as a promising solution. In this study, we aimed to enhance the yield of light olefins (ethylene, propylene, and butene) from the catalytic decomposition of low-density polyethylene (LDPE) using nano-sized SSZ-13 zeolite. SSZ-13 nanoparticles were synthesized *via* the dry gel conversion method to increase the surface area and catalytic activity. The small-pore eight-membered ring structure of SSZ-13 limits the diffusion of long-chain polyolefins, leading to LDPE cracking occurring primarily on the external surface. Compared to commercially available SSZ-13, nano-SSZ-13 exhibited a significant improvement in the decomposition activity and light olefin yield. The light olefin yield over the nano-sized SSZ-13 was *ca.* 40%, which is higher than that achieved over commercially available ZSM-5. Surface-specific ion exchange treatments clarified the role of Brønsted acid sites located on the external surface. In catalysts like SSZ-13, where reactions occur predominantly on the external surface, coke deposition inside the pores has a limited impact on diffusion, thereby suppressing catalyst deactivation. The catalyst maintained high performance over three consecutive reaction cycles without regeneration, despite the reused catalyst containing coke inside micropores, indicating that the primary active sites are located on the external surface. Moreover, SSZ-13 offers an additional advantage over other zeolites in that it can be readily reused by removing coke deposited only on its external surface. This study proposes a novel design strategy for controlling product distribution in polyolefin catalytic cracking by tuning the particle size and surface acidity of zeolites.

Sustainability spotlight

Chemical recycling is an important issue for achieving a sustainable society. Zeolites have been used as catalysts for the recovery of valuable chemicals from polymers because product distribution can be controlled by catalyst design, unlike thermal cracking. Until now, zeolites with large or medium micropores (*e.g.*, zeolite Y, zeolite beta, ZSM-5, *etc.*) have been mainly applied in polymer cracking for chemical recycling. In this work, we have demonstrated for the first time that SSZ-13 (a zeolite with small micropores) nanoparticles produce a high yield of light olefins (*ca.* 40%) on low-density polyethylene cracking. The spent SSZ-13 can be reused for 2nd and 3rd LDPE cracking without oxidative regeneration. This work shows that SSZ-13 nanoparticles are suitable as catalysts for sustainable chemical recycling technology.

1. Introduction

Approximately 400 million tons of plastic are discarded annually worldwide. In recent years, the acceleration of the SDGs and the transition toward a circular economy have made the development of plastic recycling technologies increasingly important.[1–8] This study focuses on the degradation of low-density polyethylene (LDPE), which constitutes a large portion of plastic waste.[9]

There are three major methods of plastic recycling: thermal recycling, material recycling, and chemical recycling.[10,11] Thermal recycling involves incinerating waste plastics to recover heat energy; however, it poses environmental concerns due to the high emissions of carbon dioxide. Material recycling, which involves remelting and remolding waste plastics, often results in a decline in product quality.

Consequently, chemical recycling has recently gained attention as a promising approach.[12–16] This method chemically decomposes waste plastics and converts them into other valuable chemical compounds. Among these, light olefins—such as ethylene, propylene, and butylene—are particularly valuable

[a]*Division of Chemical Engineering, Graduate School of Engineering Science, Osaka University, 1-3 Machikaneyama, Toyonaka, Osaka 560-8531, Japan. E-mail: kojimiyake@cheng.es.osaka-u.ac.jp*

[b]*Innovative Catalysis Science Division, Institute for Open and Transdisciplinary Research Initiatives (ICS-OTRI), Osaka University, Suita, Osaka 565-0871, Japan*

[c]*AC Biode Co., Ltd, 498-6 Iwakura Hanazono, Sakyo, Kyoto, 606-0024, Japan*

due to their high demand as feedstocks for products like styrene foam and PET bottles.[17–19]

Plastic pyrolysis typically occurs at high temperatures, and a key challenge lies in controlling the composition of the resulting products. Zeolites have proven to be highly effective catalysts in plastic pyrolysis.[20–22] Zeolites are porous aluminosilicates with a three-dimensional network of interconnected tetrahedral units. Their Brønsted acidity has been reported to promote the degradation of LDPE and facilitate the formation of light olefins.[23–32]

Previous studies have frequently employed beta-type and MFI-type zeolites.[33–38] Zeolites can be classified by pore size: beta-type zeolites have a pore size of approximately 0.6–0.7 nm and are categorized as large-pore zeolites, while MFI-type zeolites, with pore sizes of approximately 0.5–0.6 nm, are classified as medium-pore zeolites. The relatively large pores allow intermediate species to diffuse into the internal structure, enabling product selectivity through shape-selective catalysis.[39–42]

Among zeolites, SSZ-13, which has a pore size of 0.35–0.45 nm and falls into the category of small-pore zeolites, is considered a promising catalyst due to its strong acidity and high shape selectivity for light olefins.[43] However, no prior studies have explored the use of SSZ-13 in LDPE degradation, possibly because its small pore size limits the diffusion of the reactants and intermediates. Furthermore, since SSZ-13 has also been reported in few other reaction systems for the same reason, its application to other reaction systems is anticipated in the future.[44] Based on this, we hypothesized that the external surface of SSZ-13 plays a more significant role in the degradation reaction than its internal micropores.

In this study, we synthesized SSZ-13 nanoparticles *via* dry gel conversion with the aim of improving the yield of light olefins from LDPE pyrolysis. It has been reported that, when zeolites are employed as catalysts, a light olefin yield of approximately 40% is considered high.[45,46] By selectively using the surface of SSZ-13, we aimed to accelerate the reaction rate and evaluate both the total yield of light olefins and the catalytic durability of SSZ-13 during LDPE degradation.

2. Experimental

2.1 Synthesis of SSZ-13 using the dry gel conversion method

SSZ-13 zeolite was synthesized using a dry gel conversion method, as described in our previous literature.[47,48] Trimethyladamantylammonium hydroxide (20 wt% TMAdaOH in H_2O, SACHEM, Inc.), NaOH (Wako Pure Chemical Industries, Ltd), colloidal silica (Ludox HS-40 Sigma-Aldrich) and aluminum triisopropoxide (Nacalai Tesque, INC) were used to prepare precursor solutions. The molar ratio of the precursor solution was 25 SiO_2 : 1 Al_2O_3 : 1 Na_2O : 15 TMAdaOH. The precursor solution was stirred at room temperature for 6 h. The solution was dried at 90 °C to obtain a dried gel. The dried gel and water were transferred to an autoclave at a mass ratio of 1 : 2 and crystallized at 160 °C for 96 h under steam. The resulting powder was washed by centrifugation three times with deionized water, dried at 90 °C overnight, and calcined at 600 °C for 5 h. The synthesized zeolite was denoted as SSZ-13-DGC.

2.2 Ion exchange for SSZ-13-DGC

First, a conventional protonated SSZ-13 was prepared using a 1 mol L^{-1} NH_4Cl (FUJIFILM Wako Pure Chemical Co.) solution. The mass ratio of 1 mol L^{-1} NH_4Cl solution and SSZ-13-DGC was 30, and the mixture was stirred on a hot stirrer at 180 °C for 24 h in a Teflon container. The resulting powder was washed by centrifugation three times with deionized water, dried at 90 °C overnight, and calcined at 600 °C for 5 h. The resulting sample was denoted as SSZ-13-DGC-H. To investigate the acidity on the external surface of SSZ-13, we performed an ion exchange treatment for SSZ-13-DGC by the same procedure using tetrapropylammonium bromide (TPABr) solution instead of NH_4Cl solution. The resulting sample was denoted as SSZ-13-DGC-S-H.

As a comparison, to obtain SSZ-13 DGC without protons, SSZ-13-DGC was mixed with an aqueous NaCl solution, which became saturate at room temperature, and placed in a Teflon container and stirred on a hot stirrer at 180 °C for 24 h. The resulting powder was washed by centrifugation three times with deionized water, dried at 90 °C overnight, and calcined at 600 °C for 5 h. The resulting sample was designated as SSZ-13-DGC-Na.

2.3 Comparison with commercially available SSZ-13 and ZSM-5

Two commercial SSZ-13 zeolites with different particle sizes were purchased for comparison with SSZ-13-DGC. They are denoted as SSZ-13(1) (ACS Material) and SSZ-13(2) (Tosoh Corporation), respectively. A commercial ZSM-5 (822HOA, Tosoh, SiO_2/Al_2O_3 = 24) was used. Since the commercial product is in a protonated form, it is hereafter referred to as ZSM-5-H.

2.4 Characterization

The crystal structures of all the products were characterized by X-ray diffraction (XRD) patterns measured on a PANalytical X'Pert MPD diffractometer using Cu-Kα radiation. The morphologies and particle sizes of the samples were observed using a JEOL JCM-7000 scanning electron microscope (SEM) and a Hitachi H800 transmission electron microscope (TEM). To obtain physical information about the samples, N_2 adsorption measurements were conducted at −196 °C using a BELSORP-Max instrument (MicrotracBEL). Before the N_2 adsorption measurements, the samples were heated to 250 °C under vacuum. The acidic properties of the sample were evaluated by NH_3 temperature programmed desorption (NH_3-TPD) measurements using a BELCAT II and a BELMASS II (MicrotracBEL). The acid state in the sample was also evaluated using Fourier Transform Infrared (FT-IR) spectroscopy with pyridine (C_5H_5N) as the probe molecule.

2.5 Low density polyethylene cracking

The catalytic activity of the synthesized catalysts was evaluated by cracking of low-density polyethylene (LDPE) using thermogravimetric (TG) analysis with a DTG-60A (SHIMADZU). LDPE was manufactured by Thermo Fisher Scientific (500 microns, 0.94 g cm^{-3}). The catalyst/LDPE mixture or pure LDPE was placed in an alumina cell for thermogravimetric analysis. The mass ratio of the catalyst/LDPE mixture was fixed at 1/4.

When LDPE is cracked at elevated temperatures, it gasifies and its mass gradually decreases. In this study, "T_{half}" is defined as the temperature at which the mass of LDPE is reduced by half, and it is treated as an indicator of catalytic performance.

The catalytic performance was then evaluated by examining the LDPE cracking products. The exhaust gas generated during the cracking reaction was collected in a gas bag using a cold trap with ice water. The mass gain of the trap after the reaction was considered as the mass of the solid and liquid products, and their yields (YS + L) were calculated on a mass basis. The amount of coke deposited was evaluated using TG at a heating rate of 5 °C min^{-1} in air. The yield of product (YC) was calculated on a mass basis. The weight loss from 350 to 600 °C was attributed to the combustion of the deposited coke. The yield of gaseous products (YG) was calculated using the following equation: YG = 100 − (YS + L + YC). The yield of each gas product was analyzed using a gas chromatograph (SHIMADZU GC-2025) equipped with a flame ionization detector, and the yields of light olefins (YLO) were calculated using the following equation: YLO = YG(XC_2H_4 + XC_3H_6 + XC_4H_8), where X is the selectivity of each product.

3. Results & discussion

To confirm the crystal structures of commercial samples and SSZ-13-DGC, XRD measurements were carried out. All samples exhibited the same peaks corresponding to the CHA structure,[49,50] without any other peaks derived from some impurities, as shown in Fig. 1(a). The commercial samples and SSZ-13 had a CHA structure with high purity. To examine the effect of particle size on LDPE cracking, three samples with different particle sizes, two commercial products and SSZ-13-DGC, were compared.

Table 1 Physical properties of SSZ-13-DGC, SSZ-13(1) and SSZ-13(2)

Samples	S_{BET} [m^2 g^{-1}]	S_{ext} [m^2 g^{-1}]	Si/Al [−]	Particle size [nm]
SSZ-13(2)	558.1	1.3	13.01	2000–4000
SSZ-13(1)	434.6	18.4	5.01	1000
SSZ-13-DGC	613.0	28.6	4.17	100–150

The SEM images revealed the following order of particle sizes: SSZ-13(2) > SSZ-13(1) > SSZ-13-DGC, as shown in Fig. 1(b).

The particle size of SSZ-13 was reduced using the DGC method. It is known that the nucleation density is high and the crystal growth is suppressed during crystallization in the DGC method, leading to the formation of smaller particles.

The particle sizes of SSZ-13 (2) and SSZ-13 (1) were approximately 2–4 μm and 1 μm, respectively. TEM observation was performed to investigate the particle size of SSZ-13-DGC. Fig. 1(c) shows that the particle size of SSZ-13 was 100–150 nm. The external specific surface areas and total specific surface areas were measured by N_2 adsorption measurements, and the results are shown in Table 1. High BET surface areas were obtained due to the presence of micropores. The external surface areas of SSZ-13 increased with decreasing particle size. The Si/Al ratios were determined by EDX analysis. The ratios of SSZ-13 (1) and SSZ-13-DGC were lower than that of SSZ-13 (2).

The results of the LDPE catalytic cracking reaction test using thermogravimetry are presented in Fig. 2. The thermogravimetric results showed that the decomposition temperature decreased with decreasing particle size and increasing specific surface area. Meanwhile, there was no strong relationship between the intensity of the NH_3-TPD profiles (Fig. S1) and the LDPE half-life temperature (T_{half}) values (Table 2). Thus, it was found that the decomposition was promoted not by thermal cracking but by the reaction with the acid sites on the external surface, and that the particle size, rather than the acid sites

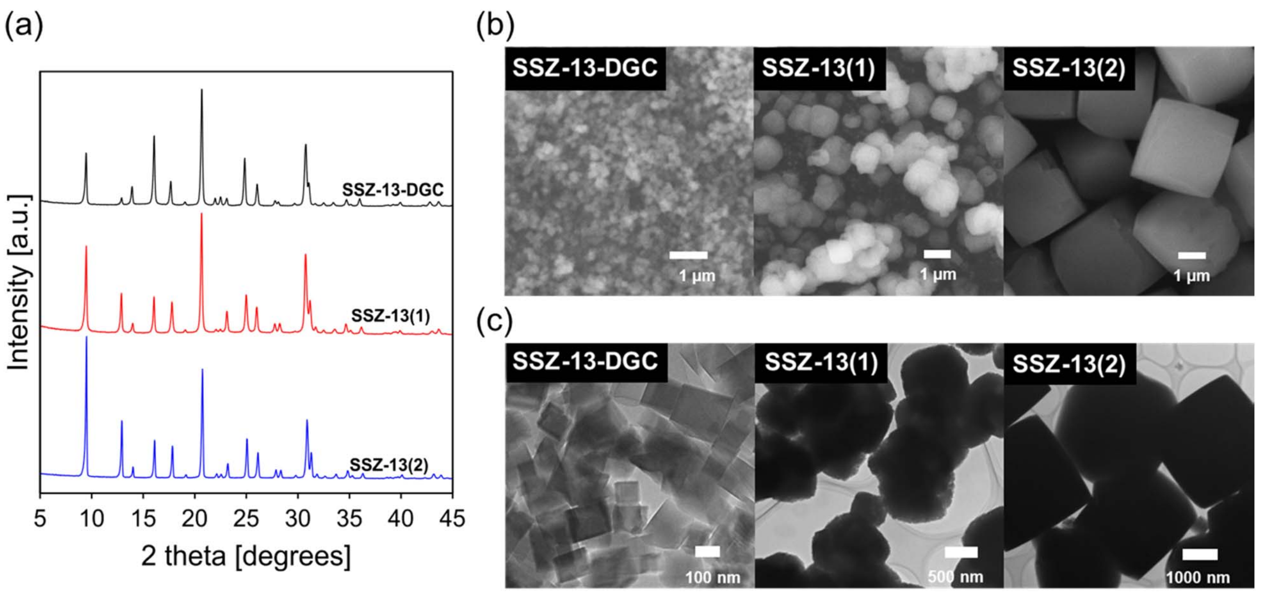

Fig. 1 (a) XRD patterns, (b) SEM images and (c) TEM images of SSZ-13-DGC, SSZ-13(1) and SSZ-13(2).

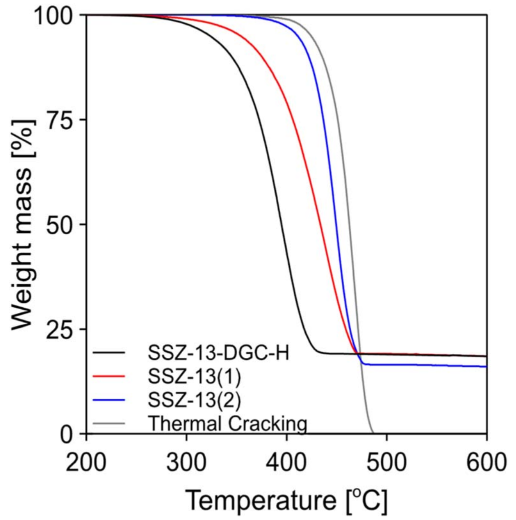

Fig. 2 TG curves obtained in the thermal cracking and the catalytic cracking of LDPE with SSZ-13-DGC-H, SSZ-13(1) and SSZ-13(2).

Table 2 T_{half} values of SSZ-13-DGC-H, SSZ-13(1), SSZ-13(2) and thermal cracking

Samples	T_{half} [°C]
SSZ-13-DGC-H	394
SSZ-13(1)	433
SSZ-13(2)	449
Thermal cracking	462

inside the micropores, contributed to the decomposition temperature. GC was used to analyze the product distribution during LDPE cracking with and without the catalysts. First, the selectivities of gas, liquid + wax, and coke were calculated using a mass balance (Fig. 3(a)). The gas yield increased with decreasing particle size and increasing specific surface area. The detailed distributions of the gaseous products were analyzed using GC, as shown in Fig. 3(b). The yields of light olefins for each sample are also shown in Fig. 3(c). There was a significant difference in product distribution in gas. The gas yield increased with decreasing particle size, and the yield of light olefins also increased. Additionally, LDPE decomposition reaction tests were conducted by adjusting the catalyst amount to achieve the same Al content as LDPE based on the Si/Al ratio (Fig. S2 and S3). These results further confirm the significant influence of particle size.

Next, to elucidate the role of the external surface in the LDPE degradation reaction, we compared SSZ-13-DGC-S-H, which is proton-exchanged only on the external surface of SSZ-13-DGC, and SSZ-13-DGC-Na, which has no acid sites by Na ion exchange (Scheme 1). There was no particular change in particle size before and after ion exchange (Fig. S4).

In zeolite catalysts, two peaks are generally observed, with the high-temperature side said to originate from Brønsted acids.[51] The NH_3-TPD measurement results shown in Fig. 4(a) confirm that the overall Brønsted acid amount has decreased in SSZ-13-DGC-S-H and SSZ-13-DGC-Na compared to SSZ-13-DGC, as evidenced by the reduction in peak intensity by approximately 500–600 °C. Next, we measured FT-IR spectra with pyridine as a probe molecule. The pyridine molecule has a kinetic diameter (0.57 nm),[52–55] which is larger than the micropore size of SSZ-13 zeolites. Since pyridine cannot penetrate into the micropores of SSZ-13, this measurement can be used to evaluate the acidity on the external surface of SSZ-13 zeolites.[26] A Brønsted acid peak is observed at 1580 cm^{-1} in FT-IR measurements using pyridine.[56] Therefore, based on the FT-IR measurement results shown in Fig. 4(b), we confirmed the introduction of Brønsted acid in the order of SSZ-13-DGC and SSZ-13-DGC-S-H. In the case of SSZ-13-DGC-Na, although a similar peak appears to be present, it is smaller compared to the others, indicating that it does not possess Brønsted acid sites. Combining these results with the NH_3-TPD measurement results, it is inferred that only the surface of SSZ-13-DGC-S-H underwent proton exchange.

GC was used to analyze the product distribution during LDPE cracking with and without the catalysts. First, the selectivities of gas, liquid + wax, and coke were calculated with a mass balance

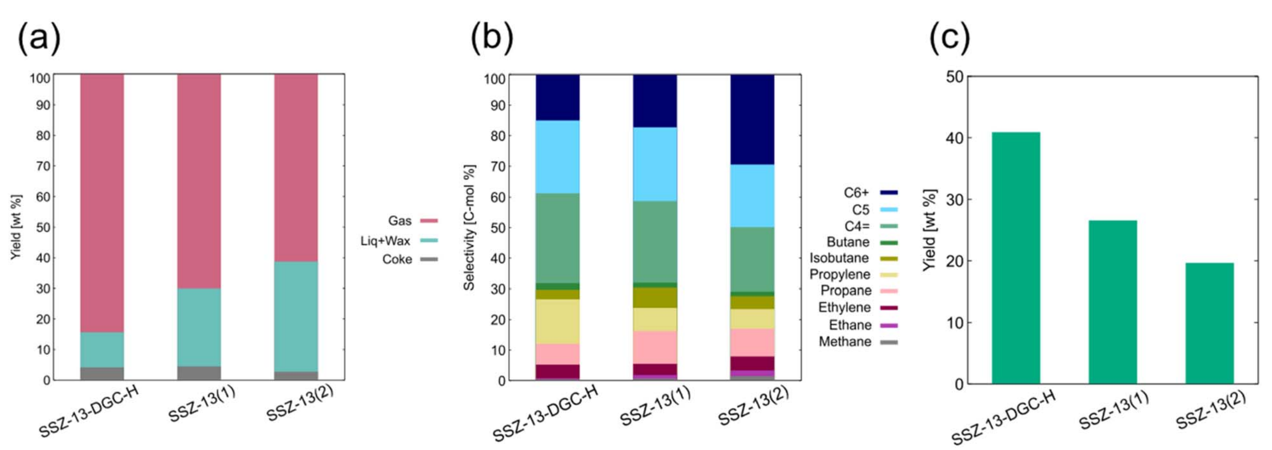

Fig. 3 (a) Yields for each phase, (b) gas product distribution and (c) yield for light olefins (ethylene + propylene + butene) in catalytic cracking of LDPE over SSZ-13-DGC-H, SSZ-13(1) and SSZ-13(2).

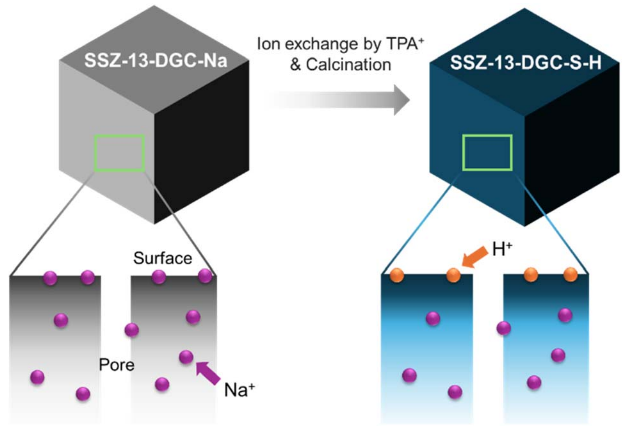

Scheme 1 Preparation method of SSZ-13-DGC-S-H.

(Fig. 5(a)). The detailed distributions of the gaseous products were analyzed using GC, as shown in Fig. 5(b). The yields of light olefins for each sample are also shown in Fig. 5(c).

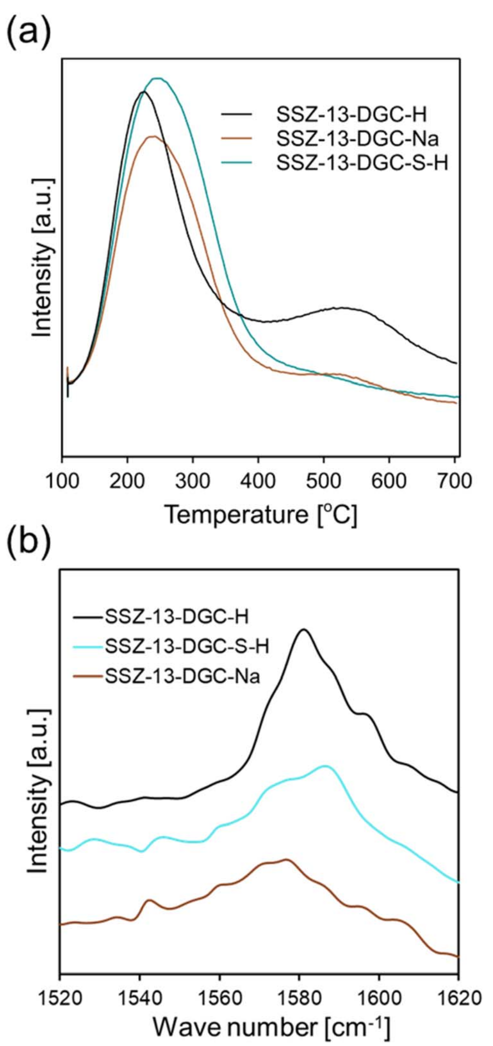

Fig. 4 (a) NH_3-TPD profiles and (b) FT-IR spectra of SSZ-13-DGC-H, SSZ-13-DGC-S-H and SSZ-13-DGC-Na.

In SSZ-13-DGC-Na, the reaction was assumed to have made little progress because of the lack of an acid point, given the high liquid yield. In SSZ-13-DGC and SSZ-13-DGC-S-H, the yields of C4 olefins were both high; since the pore size of SSZ-13 is suitable for C2 and C3 olefins, we can assume that the reaction proceeds mainly on the external surface rather than by shape selectivity inside the pore. In addition, the difference in the yield of light olefins between SSZ-13-DGC-H and SSZ-13-DGC-S-H is attributed to the difference in the number of acid sites on the external surface. As shown in Fig. 4, this is because the bulky tetrapropylammonium ions cannot fully exchange protons on all external surface sites.

The catalysts containing coke after the LDPE decomposition reaction of SSZ-13-DGC-H and SSZ-13-DGC-S-H were named SSZ-13-DGC-H-coke and SSZ-13-DGC-S-H-coke, respectively. From the adsorption isotherms of SSZ-13-DGC-H-coke and SSZ-13-DGC-S-H-coke, it can be inferred that the coke blocks the pores in the same way (Fig. S5). SSZ-13-DGC-H-coke and SSZ-13-DGC-S-H-coke show similar values in S_{bet} and S_{ext}, respectively (Table S1). This suggests that coke precipitates in the same location and amount inside the pores and on the surface of SSZ-13.

From the discussion so far, it is clear that the reaction proceeds mainly on the external surface of SSZ-13 in the LDPE decomposition reaction, while ZSM-5 and other catalysts use the inside of the pore as the reaction field. As the LDPE decomposition reaction proceeds, coke is deposited inside the pore and diffusion in the pore becomes limited, leading to deactivation. Therefore, we believe that the SSZ-13 catalyst, whose reaction field is mainly on the external surface, was considered to be resistant to repeated use without being affected by coke deposition. So, we repeated the LDPE decomposition reaction test three times using ZSM-5-H. (The characterization data of ZSM-5-H is shown in Fig. S6 and Table S2.)

The detailed results are summarized in Fig. 6. The result of the first reaction test is indicated as SSZ-13-DGC-H-1st. (This refers to the same sample as SSZ-13-DGC-H.) The second and third samples used repeatedly are denoted as SSZ-13-DGC-2nd and SSZ-13-DGC-3rd, respectively. The catalyst after the first reaction was directly used without any regeneration processes, which means that the coke-deposited catalysts were used directly for the second and third reactions. The second and third reactions were subsequently performed in the same manner, using four times the LDPE-to-catalyst mass ratio. In the first reaction (Fig. 6), SSZ-13-DGC exhibited higher coke deposition and light olefin yield than ZSM-5. In addition, SSZ-13-DGC produced ethylene, whereas ZSM-5 did not produce ethylene. Based on the currently available data and the lack of alternative analytical methods at this stage, these results imply that a part of the reaction may occur inside the micropores of the CHA structure, although the reaction occurs mainly on the external surface. Then, almost all reactants that entered into the micropores were converted into coke due to the excess reactions caused by low diffusivity inside the small micropores. Meanwhile, a reaction benefiting from the shape selectivity partially occurred, resulting in the production of ethylene over SSZ-13-DGC. Additionally, SSZ-13 exhibited a higher propane yield than ZSM-5. The hydrogen transfer reaction[57,58] should be

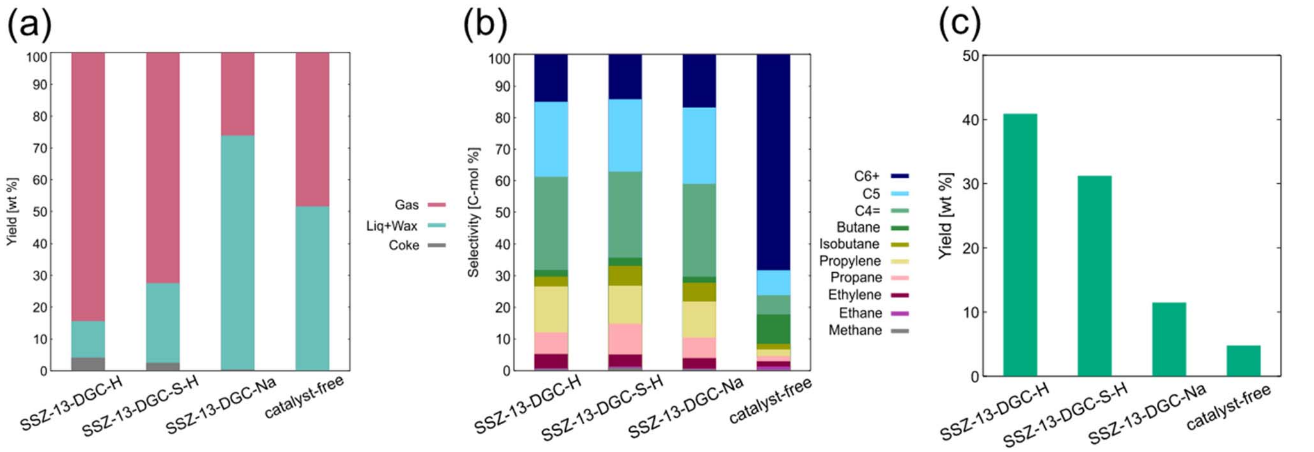

Fig. 5 (a) Yields for each phase, (b) gas product distribution and (c) yield for light olefins (ethylene + propylene + butene) in catalytic cracking of LDPE catalyst-free and over SSZ-13-DGC-H, SSZ-13-DGC-S-H and SSZ-13-DGC-Na.

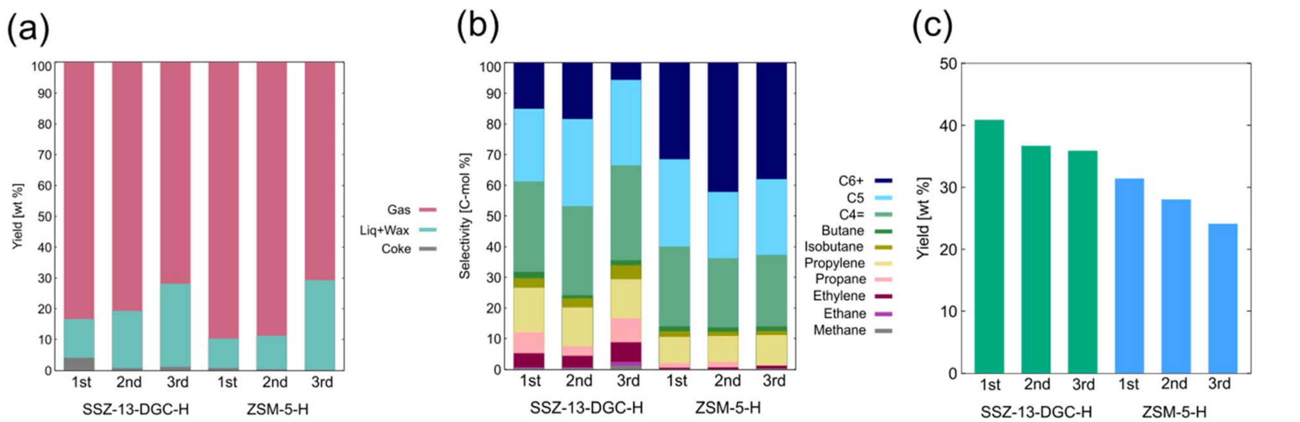

Fig. 6 (a) Yields for each phase, (b) gas product distribution and (c) yield for light olefins obtained in repeated catalytic cracking of LDPE over SSZ-13-DGC-H and ZSM-5-H.

promoted due to the higher acidity and smaller micropores than ZSM-5. In the second reaction, the catalytic performance was maintained although SSZ-13-DGC has a large amount of coke (16.7 wt%: the mass ratio of deposited coke and catalyst was analyzed using thermogravimetric analysis), indicating that the main reaction occurred on the external surface because the micropores are blocked by coke. Ethylene was produced even in the second reaction as for SSZ-13-DGC, implying that shape selectivity was not completely lost. It may be thought that micropores near the external surface were not blocked by coke because micropore adsorption was not lost completely according to N_2 adsorption isotherms (Fig. S3). This may be because the diffusivity in the micropores near the external surface is higher than that in the micropores in the deep region inside the particles. The micropores near the external surface induced the shape selectivity of the CHA structure, leading to the production of ethylene even in the second reaction over the SSZ-13-DGC. In the third reaction, SSZ-13-DGC showed a similar light olefin yield, and SSZ-13-DGC showed higher light olefin yields than ZSM-5 from the first to the third reaction (Fig. 6(c)). Thus, SSZ-13-DGC is an effective catalyst for producing light olefins by LDPE cracking. In contrast, the liquid yield increased with an increase in the cycle number. This is because acid sites on the external surface were partially covered by coke with an increase in the cycle number. In addition, although the decrease was slight, the yield of light olefins also decreased for SSZ-13-DGC compared to ZSM-5-H. This may be due to the coke partially covering the acid sites on the external surface, reducing the activity of the decomposition reaction. However, SSZ-13 is less susceptible to coke deposition, since the reaction occurs mainly on its external surface as discussed above. In this experiment, it maintained a light-olefin yield of more than 36% up to the third cycle. Due to this characteristic, it can be considered that the nano-sized SSZ-13 is useful for the production of light olefins even in its unmodified form, compared to other zeolites.[46] In terms of catalyst regeneration, ZSM-5 requires the removal of coke inside the pores, whereas SSZ-13 requires the removal of coke only on the external surface; therefore, it is assumed that catalyst regeneration can be performed at lower temperatures.

4. Conclusions

Nano-sized SSZ-13 zeolites were synthesized *via* the dry gel conversion method, and they exhibited excellent catalytic performance in the decomposition of LDPE. These zeolites possess a CHA-type framework, small particle size (100–150 nm), and a high external surface area, which together enhance catalytic activity by exposing more accessible acid sites. NH_3-TPD and pyridine-FTIR analyses confirmed that Brønsted acid sites on the external surface play a crucial role in promoting LDPE decomposition. When protons of the acid sites were exchanged with Na ions, catalytic activity declined significantly, highlighting their importance. The nano-SSZ-13 catalyst effectively lowered the decomposition temperature of LDPE and increased the gas yield, particularly for light olefins such as ethylene and propylene. Reaction tests further demonstrated that reducing the particle size and increasing the external surface area contribute to improved light olefin yields, achieving a high yield of 40%. The catalytic reaction was found to occur predominantly on the external surface, with limited contribution from internal micropores. Despite coke formation during repeated use, the catalyst maintained high activity over three cycles without regeneration. In contrast, ZSM-5 exhibited rapid deactivation due to pore blockage by coke. Moreover, compared with other zeolites, SSZ-13 offers the advantage of maintaining high catalytic performance by simply removing coke deposited on its external surface. These findings demonstrate that nano-structured SSZ-13 is a highly active and stable catalyst for the efficient conversion of LDPE into valuable light olefins.

Author contributions

Yoshiki Murata: conceptualization, investigation, visualization, writing – original draft. Ryuga Nakai: investigation, writing – review & editing. Koji Miyake: conceptualization, supervision, visualization, methodology, writing – review & editing. Yoshiaki Uchida: writing – review & editing. Atsushi Mizusawa: writing – review & editing. Tadashi Kubo: writing – review & editing. Norikazu Nishiyama: supervision, resources, writing – review & editing.

Conflicts of interest

There are no conflicts to declare.

Data availability

The data supporting this article have been included as part of the supplementary information (SI). Supplementary information is available. See DOI: https://doi.org/10.1039/d5su00602c.

Acknowledgements

A part of the present experiments was carried out by using a facility in the Research Center for Ultra-High Voltage Electron Microscopy, Osaka University.

Notes and references

1 T. Thiounn and R. C. Smith, *J. Polym. Sci.*, 2020, **58**, 1347–1364.
2 A. L. Andrady and M. A. Neal, *Philos. Trans. R. Soc., B*, 2009, **364**, 1977–1984.
3 R. Qi, D. L. Jones, Z. Li, Q. Liu and C. Yan, *Sci. Total Environ.*, 2020, **703**, 134722.
4 C. M. Rochman, M. A. Browne, B. S. Halpern, B. T. Hentschel, E. Hoh, H. K. Karapanagioti, L. M. Rios-Mendoza, H. Takada, S. Teh and R. C. Thompson, *Nature*, 2013, **494**, 169–171.
5 H. Li, H. A. Aguirre-Villegas, R. D. Allen, X. Bai, C. H. Benson, G. T. Beckham, S. L. Bradshaw, J. L. Brown, R. C. Brown, V. S. Cecon, J. B. Curley, G. W. Curtzwiler, S. Dong, S. Gaddameedi, J. E. García, I. Hermans, M. S. Kim, J. Ma, L. O. Mark, M. Mavrikakis, O. O. Olafasakin, T. A. Osswald, K. G. Papanikolaou, H. Radhakrishnan, M. A. S. Castillo, K. L. Sánchez-Rivera, K. N. Tumu, R. C. V. Lehn, K. L. Vorst, M. M. Wright, J. Wu, V. M. Zavala, P. Zhou and G. W. Huber, *Green Chem.*, 2022, **24**, 8899–9002.
6 J. R. Jambeck, R. Geyer, C. Wilcox, T. R. Siegler, M. Perryman, A. Andrady, R. Narayan and K. L. Law, *Science*, 2015, **347**, 768–771.
7 A. K. Panda, R. K. Singh and D. K. Mishra, *Renewable Sustainable Energy Rev.*, 2010, **14**, 233–248.
8 E. Sanniyasi, R. K. Gopal, D. K. Gunasekar and P. P. Raj, *Sci. Rep.*, 2021, **11**, 17233.
9 H. Raghav, B. Joshi, K. D. P. L. Kumar, S. Kumar and B. Sarkar, *J. Environ. Chem. Eng.*, 2025, **13**, 115254.
10 K. Ragaert, L. Delva and K. Van Geem, *Waste Manage.*, 2017, **69**, 24–58.
11 J. Hopewell, R. Dvorak and E. Kosior, *Philos. Trans. R. Soc., B*, 2009, **364**, 2115–2126.
12 G. Martínez-Narro, S. Hassan and A. N. Phan, *J. Environ. Chem. Eng.*, 2024, **12**, 112323.
13 X. Chen, L. Cheng, J. Gu, H. Yuan and Y. Chen, *Chem. Eng. J.*, 2024, **479**, 147853.
14 R. A. Clark and M. P. Shaver, *Chem. Rev.*, 2024, **124**, 2617–2650.
15 H. Luo, H. Tyrrell, J. Bai, R. I. Muazu and X. Long, *Green Chem.*, 2024, **26**, 11444–11467.
16 A. Schade, M. Melzer, S. Zimmermann, T. Schwarz, K. Stoewe and H. Kuhn, *ACS Sustainable Chem. Eng.*, 2024, **12**, 12270–12288.
17 C. P. Nicholas, *Appl. Catal., A*, 2017, **543**, 82–97.
18 K. P. de Jong, *Science*, 2016, **351**, 1030–1031.
19 M. Fakhroleslam and S. M. Sadrameli, *Ind. Eng. Chem. Res.*, 2020, **59**, 12288–12303.
20 J. Zhang, X. Wang, K. Sun, T. Wang, H. Zhao, X. Chen, X. Zhang and C. Yang, *ChemistrySelect*, 2025, **10**, e202405627.
21 J. Aguado, D. P. Serrano, G. S. Miguel, J. M. Escola and J. M. Rodríguez, *J. Anal. Appl. Pyrolysis*, 2007, **78**, 153–161.
22 Y. Wang, Y. Zhang, H. Fan, P. Wu, M. Liu, X. Li, J. Yang, C. Liu, P. Bai and Z. Yan, *Catal. Today*, 2022, **405–406**, 135–143.

23 B. Xu, C. Sievers, S. B. Hong, R. Prins and J. A. van Bokhoven, *J. Catal.*, 2006, **244**, 163–168.
24 J. Aguado, D. P. Serrano, J. M. Escola and A. Peral, *J. Anal. Appl. Pyrolysis*, 2009, **85**, 352–358.
25 S. Kokuryo, K. Miyake, Y. Uchida, A. Mizusawa, T. Kubo and N. Nishiyama, *Mater. Today Sustain.*, 2022, **17**, 100098.
26 S. Tsubota, S. Kokuryo, K. Tamura, K. Miyake, Y. Uchida, A. Mizusawa, T. Kubo and N. Nishiyama, *Catal. Sci. Technol.*, 2024, **14**, 1369–1374.
27 L. Dai, N. Zhou, K. Cobb, P. Chen, Y. Wang, Y. Liu, R. Zou, H. Lei, B. A. Mohamed, Y. Cheng and R. Ruan, *Appl. Catal., B*, 2022, **318**, 121835.
28 L. Quesada, M. Calero de Hoces, M. A. Martín-Lara, G. Luzón and G. Blázquez, *Sustainability*, 2020, **12**, 5482.
29 R. Miandad, M. A. Barakat, M. Rehan, A. S. Aburiazaiza, I. M. I. Ismail and A. S. Nizami, *Waste Manage.*, 2017, **69**, 66–78.
30 W. U. Eze, R. Umunakwe, H. C. Obasi, M. I. Ugbaja, C. C. Uche, I. C. Madufor, W. U. Eze, R. Umunakwe, H. C. Obasi, M. I. Ugbaja, C. C. Uche and I. C. Madufor, *CTR*, 2021, **1**, 50–69.
31 K. Li, J. Valla and J. Garcia-Martinez, *ChemCatChem*, 2014, **6**, 46–66.
32 S. Kokuryo, K. Tamura, S. Tsubota, K. Miyake, Y. Uchida, A. Mizusawa, T. Kubo and N. Nishiyama, *Catal. Sci. Technol.*, 2024, **14**, 3589–3595.
33 A. Marcilla, A. Gómez-Siurana and F. Valdés, *J. Anal. Appl. Pyrolysis*, 2007, **79**, 433–442.
34 K. Pyra, K. A. Tarach, D. Majda and K. Góra-Marek, *Catal. Sci. Technol.*, 2019, **9**, 1794–1801.
35 T. Liu, Y. Li, Y. Zhou, S. Deng and H. Zhang, *Catalysts*, 2023, **13**, 382.
36 S. Kokuryo, K. Tamura, K. Miyake, Y. Uchida, A. Mizusawa, T. Kubo and N. Nishiyama, *Catal. Sci. Technol.*, 2022, **12**, 4138–4144.
37 Y. Li, T. Liu, S. Deng, X. Liu, Q. Meng, M. Tang, X. Wu and H. Zhang, *Catalysts*, 2024, **14**, 78.
38 J. P. Hittinger and D. F. Shantz, *Microporous Mesoporous Mater.*, 2022, **343**, 112170.
39 D. P. Serrano, J. Aguado and J. M. Escola, *Ind. Eng. Chem. Res.*, 2000, **39**, 1177–1184.
40 *Catalytic Degradation of High-Density Polyethylene over Different Zeolitic Structures*, https://www.researchgate.net/publication/231393792_Catalytic_Degradation_of_High-Density_Polyethylene_over_Different_Zeolitic_Structures, accessed July 3, 2025.
41 Y. Wang, Y. Zhang, H. Fan, P. Wu, M. Liu, X. Li, J. Yang, C. Liu, P. Bai and Z. Yan, *Catal. Today*, 2022, **405–406**, 135–143.
42 M. M. Hasan, N. Batalha, G. Fraga, M. H. M. Ahmed, L. Pinard, M. Konarova, S. Pratt and B. Laycock, *Sustainable Energy Fuels*, 2022, **6**, 1587–1602.
43 S. S. R. Putluru, L. Schill, A. D. Jensen and R. S. N. Fehrmann, *J. Chem.*, 2018, 8614747.
44 H. Li, S. Yang, A. Riisager, A. Pandey, R. S. Sangwan, S. Saravanamurugan and R. Luque, *Green Chem.*, 2016, **18**, 5701–5735.
45 Y. Li, T. Liu, S. Deng, X. Liu, Q. Meng, M. Tang, X. Wu and H. Zhang, *Catalysts*, 2024, **14**, 78.
46 S. Kokuryo, S. Tsubota, K. Miyake, Y. Uchida, A. Mizusawa, T. Kubo and N. Nishiyama, *Adv. Sustainable Syst.*, 2025, **9**, 2400625.
47 H. Al Jabri, K. Miyake, K. Ono, M. Nakai, R. Inoue, Y. Hirota, Y. Uchida, Y. Wang, T. Nishitoba, T. Yokoi, T. Ohnishi, M. Ogura and N. Nishiyama, *Microporous Mesoporous Mater.*, 2020, **297**, 109780.
48 H. Al Jabri, K. Miyake, K. Ono, M. Nakai, Y. Hirota, Y. Uchida, M. Miyamoto and N. Nishiyama, *Microporous Mesoporous Mater.*, 2019, **278**, 322–326.
49 M. A. Deimund, L. Harrison, J. D. Lunn, Y. Liu, A. Malek, R. Shayib and M. E. Davis, *ACS Catal.*, 2016, **6**, 542–550.
50 Y. Wang, C. Wang, J. Wang, J. Wang, L. Wang, C. Xu and M. Shen, *Materials*, 2020, **13**, 1829.
51 L. Rodríguez-González, F. Hermes, M. Bertmer, E. Rodríguez-Castellón, A. Jiménez-López and U. Simon, *Appl. Catal., A*, 2007, **328**, 174–182.
52 J. Přech, P. Pizarro, D. P. Serrano and J. Čejka, *Chem. Soc. Rev.*, 2018, **47**, 8263–8306.
53 R. Feng, X. Yan, X. Hu, Y. Wang, Z. Li, K. Hou and J. Lin, *J. Porous Mater.*, 2018, **25**, 1743–1756.
54 V. Zholobenko, C. Freitas, M. Jendrlin, P. Bazin, A. Travert and F. Thibault-Starzyk, *J. Catal.*, 2020, **385**, 52–60.
55 D. Hartanto, L. S. Yuan, S. M. Sari, D. Sugiarso, I. K. Murwarni, T. Ersam, D. Prasetyoko and H. Nur, *J. Teknol. Lab.*, 2016, **78**(6), 223–228.
56 *The Role of Bronsted and Lewis Acidity in the Green Synthesis of Homopropargyl Alcohols over HZSM-5*, https://scielo.org.za/scielo.php?script=sci_arttext&pid=S0379-43502018000100008&lng=en&nrm=iso&tlng=en, accessed July 3, 2025.
57 Z. Guo, Q. Chen, J. Liu and B. Yang, *Nat. Commun.*, 2025, **16**, 1152.
58 A. E. Enss, P. Huber, P. N. Plessow and F. Studt, *J. Phys. Chem. C*, 2024, **128**, 15367–15379.